OXFORD

Human Molecular Genetics, 2015, Vol. 24, No. 25 7159–7170

doi: 10.1093/hmg/ddv384
Advance Access Publication Date: 16 September 2015
Original Article

ORIGINAL ARTICLE

Abnormalities of motor function, transcription and cerebellar structure in mouse models of *THAP1* dystonia

Marta Ruiz[1,†], Georgina Perez-Garcia[3,†], Maitane Ortiz-Virumbrales[3], Aurelie Méneret[2], Andrika Morant[3], Jessica Kottwitz[3], Tania Fuchs[3], Justine Bonet[3], Pedro Gonzalez-Alegre[5], Patrick R. Hof[4], Laurie J. Ozelius[2,3] and Michelle E. Ehrlich[1,2,3,*]

[1]Department of Pediatrics, [2]Department of Genetics and Genomic Sciences, [3]Department of Neurology, [4]Department of Neurosciences, Icahn School of Medicine at Mount Sinai, New York, NY 10029, USA and [5]Department of Neurology, University of Iowa Hospitals and Clinics, Iowa City, IA 52242, USA

*To whom correspondence should be addressed at: Annenberg Pavilion Room 14-44, Icahn School of Medicine at Mount Sinai, 1 Gustave L. Levy Place, New York, NY 10029, USA. Tel: +1 2122419270; Fax: +1 2122413406; Email: michelle.ehrlich@mssm.edu

Abstract

DYT6 dystonia is caused by mutations in *THAP1* [Thanatos-associated (THAP) domain-containing apoptosis-associated protein] and is autosomal dominant and partially penetrant. Like other genetic primary dystonias, DYT6 patients have no characteristic neuropathology, and mechanisms by which mutations in *THAP1* cause dystonia are unknown. Thap1 is a zinc-finger transcription factor, and most pathogenic *THAP1* mutations are missense and are located in the DNA-binding domain. There are also nonsense mutations, which act as the equivalent of a null allele because they result in the generation of small mRNA species that are likely rapidly degraded via nonsense-mediated decay. The function of Thap1 in neurons is unknown, but there is a unique, neuronal 50-kDa Thap1 species, and Thap1 levels are auto-regulated on the mRNA level. Herein, we present the first characterization of two mouse models of DYT6, including a pathogenic knockin mutation, C54Y and a null mutation. Alterations in motor behaviors, transcription and brain structure are demonstrated. The projection neurons of the deep cerebellar nuclei are especially altered. Abnormalities vary according to genotype, sex, age and/or brain region, but importantly, overlap with those of other dystonia mouse models. These data highlight the similarities and differences in age- and cell-specific effects of a *Thap1* mutation, indicating that the pathophysiology of *THAP1* mutations should be assayed at multiple ages and neuronal types and support the notion of final common pathways in the pathophysiology of dystonia arising from disparate mutations.

Introduction

Little is known regarding the pathogenic molecular mechanisms underlying the abnormal, painful muscle contractions characteristic of primary dystonia (1). Medical and surgical treatments of the dystonias are symptomatic and are not always of lasting benefit. DYT6 is an autosomal dominant and partially penetrant. DYT6 patients lack any characteristic neuropathologic lesion; however, neuroimaging in manifesting and non-manifesting carriers (NMCs) demonstrates abnormalities in the cerebello-thalamo-cortical and cortico-striato-pallido-thalamo-cortical pathways (2). DYT6 is caused by mutations in *THAP1* [Thanatos-associated (THAP) domain-containing apoptosis-associated protein] (1,3). Thap1 is a zinc-finger transcription factor, featuring an N-terminus DNA-binding domain (DBD), a nuclear localization signal and a coiled-coiled domain toward the C-terminus (4,5). Most pathogenic *THAP1* mutations are missense and are

[†]M.R. and G.P.-G. contributed equally to this work.

Received: April 28, 2015. **Revised and Accepted:** September 14, 2015

located in the DBD, but mutations occur in other domains as well. Some mutations are nonsense, resulting in small mRNA species likely subject to rapid decay, yielding the equivalent of a null allele (3).

Little is also known about the role or targets of Thap1 in neurons, but in other cell types, the protein has pro-apoptotic activity and is implicated in proliferation via regulation of pRB-E2F pathway genes (5–8). Up-regulation and down-regulation of Thap1 leads to similar phenotypes in human umbilical vein endothelial cells (HUVECs) (7). In a neuronal cell line, overexpression of Thap1 decreases endogenous *THAP1* mRNA, and in induced pluripotent stem cells derived from patients with a *THAP1* mutation, *THAP1* mRNA is up-regulated (9). These observations lead to the conclusion that *THAP1* levels are auto-regulated at the transcriptional level.

Thap1 is a member of a large protein family (5,10,11) without homology to other proteins implicated in dystonia. There are shared clinical features among the primary torsion dystonias although there are differences in ages of presentation and in anatomic distribution (1), and a major research focus is to identify common pathophysiologic mechanisms. Clinical and animal studies suggest the existence of structural and molecular pathogenic features that are common to several genetic dystonias. These include the involvement of the cortico-striato-pallido-thalamo-cortical and cerebello-thalamo-cortical pathways, impairment in dopaminergic and cholinergic neurotransmission, abnormalities of cell cycle and endoplasmic reticulum stress pathways and transcriptional dysregulation (1,12,13).

To study the effects of *THAP1* mutations in mouse neurons, we created and initiated the characterization of mice expressing C54Y *THAP1*, a disease-causing mutation in one of the three cysteine residues that are part of the zinc binding motif ($CysX_{2-4}CysX_{35-53}CysX_2His$) (5). We created two lines of mice with physiologic mutations, a *Thap1*^{C54Y} knockin (KI) mouse and a mouse with a null allele. The C54Y mutation prevents binding of Thap1 to DNA *in vitro* (3,14). In particular, we sought to determine whether Thap1 function is associated with the pathways and systems heretofore linked with dystonia. Thus, we (1) compare brain anatomy and motor function in the two recombinant mouse strains; (2) measure baseline tissue monoamine levels; (3) compare downstream regulation of reported Thap1 targets, including *Thap1* itself (7,9), *Rrm1* (7) and *Tor1a* (9,14,15); (4) perform targeted assays of gene expression in pathways hypothesized to contribute to primary dystonia pathophysiology, including neurotransmitter pathways and genes with a role in plasticity.

Results

Generation and identification of *Thap1*-recombinant mice

We generated two *THAP1*/DYT6 genetically modified mouse alleles, including (1) *Thap1*^{C54Y}, a constitutive KI of the C54Y causative mutation in the DBD of *THAP1* and (2) *Thap1*$^{-}$, a constitutive null, or knockout (KO), allele. The *THAP1* gene structure is shown in Figure 1A, and the targeting construct in Figure 1B. Southern blot analysis of a wild-type (WT) and *Thap1*^{C54Y} heterozygote mouse is shown in Figure 1C. The constitutive null allele was derived by crossing *Thap1*$^{C54Y/+}$ with a line in which the CMV promoter directs Cre recombinase expression in germ cells (16). Heterozygotes of each genotype were produced in Mendelian ratios and were viable and fertile. Almost all *Thap1*$^{-/-}$ and *Thap1*$^{C54Y/-}$ embryos died by E10, but there were rare survivors up to E14. We did not obtain any *Thap1*$^{C54Y/C54Y}$ embryos at those ages. *Thap1*$^{-/-}$ and *Thap1*$^{C54Y/-}$ embryos were smaller than WT or heterozygote littermates, and variable defects were externally obvious, including absence of eyes and liver (Fig. 1D). Transillumination revealed a marked decrease in brain tissue and relative increase in ventricular volume (Fig. 1E). Tuj1-immunopositive 'neurons' in *Thap1*$^{-/-}$ and *Thap1*$^{C54Y/-}$ embryos were few in number and of unusual morphology without obvious processes (*Thap1*$^{C54Y/-}$ pictured in Fig. 1F), suggesting a role for Thap1 in multiple stages of neuronal differentiation. Further study of the embryos and their neuronal development is ongoing.

The adult brains of the two heterozygote genotypes, *Thap1*$^{C54Y/+}$ and *Thap1*$^{+/-}$, appeared similar in appearance, size (Fig. 1G) and weight when compared with each other and the WT (WT = 0.50 g ± 0.03 SEM; KI/+ = 0.53 g ± 0.04; KO = 0.52 g ± 0.04).

Projection neurons in the dentate nucleus of the cerebellum (DNC) are abnormal in *THAP1*$^{C54Y/+}$ and *THAP1*$^{+/-}$ mice

We examined early postnatal regionalization and expression of neuronal subtype-specific markers in *Thap1*$^{C54Y/+}$ male mice (Supplementary Material, Fig. S1A), with particular attention to regions implicated in dystonia. In summary, we saw no obvious difference following Nissl stain of the adult and P1 striatum, and neither immunostaining for DARPP-32 (dopamine and cyclic-AMP-regulated phosphoprotein 32 kDa) nor mu opiate receptor (MOR) revealed changes. Nissl stain of the P1 and adult cortex, with special attention to the somatosensory cortex, appeared normal. Similarly, immunocytochemistry for glial fibrillary acidic protein, a marker of reactive gliosis, was unchanged from controls in both forebrain and hindbrain. The striatum in adult *Thap1*$^{+/-}$ adult male mice also appeared grossly normal as determined by Nissl, anti-DARPP-32 and anti-MOR staining (Supplementary Material, Fig. S1C).

In the adult *Thap1*$^{C54Y/+}$ male mice, cerebellar folia were grossly normal (Fig. 2Aa and a′), but the adult and P1 DNC appeared different, i.e. hypocellular, relative to the WT mouse as visualized by both Nissl (a, a′, b, b′) and immunostaining for Tbr1 (c, c′), a transcription factor highly expressed in embryonic and early postnatal period in cerebellum and neocortex (17,18). The immunostaining for Tbr1 in the P1 cortex appeared normal (d, d′). Thus, we more closely examined the DNC in the presence of a KI or null allele in the adult. In the adult *Thap1*$^{C54Y/+}$, we observed hypocellularity in the dentate, i.e. lateral, nucleus (Fig. 2Bb and f), but this difference appeared more obvious in the *Thap1*$^{+/-}$ (d and h) than in the *Thap1*$^{C54Y/+}$. We therefore counted the large neurons in the DNC, most of which are glutamatergic and GABAergic projection neurons (18,19) in adult *Thap1*$^{+/-}$ and *Thap1*$^{C54Y/+}$ mice, each with its own set of controls. There was a 40% decrease in cell number in 6-month-old *Thap1*$^{+/-}$ mice ($n = 5$ of each genotype; *Thap1*$^{+/+}$ = 2037 ± 133; *Thap1*$^{+/-}$ = 1233 ± 216; one-way ANOVA, $P = 0.013$) (Fig. 2C). In 6-month-old *Thap1*$^{C54Y/+}$ mice, there was only a slight trend toward a decrease in cell number ($n = 5$ of each genotype; *Thap1*$^{+/+}$ = 2216 ± 133 S.D.; *Thap1*$^{C54Y/+}$ = 1873 ± 157 S.D.; $P = 0.134$) (Fig. 2C). There was, however, a 40% increase in soma volume in *Thap1*$^{C54Y/+}$ relative to *Thap1*$^{+/+}$ [*Thap1*$^{+/+}$ 4976 ± 1089, S.D. versus *Thap1*$^{C54Y/}$ 7580 ± 914, S.D. (μm^3), $P < 0.0001$] (Fig. 2D), whereas soma volume was normal in *Thap1*$^{+/-}$.

Thap1$^{C54Y/+}$ and *Thap1*$^{+/-}$ mice display abnormalities of motor function

On visual inspection in their home cages up to 18 months of age, *Thap1*$^{C54Y/+}$ and *Thap1*$^{+/-}$ mice did not display overt abnormalities, nor did they display forelimb or hind limb clasping

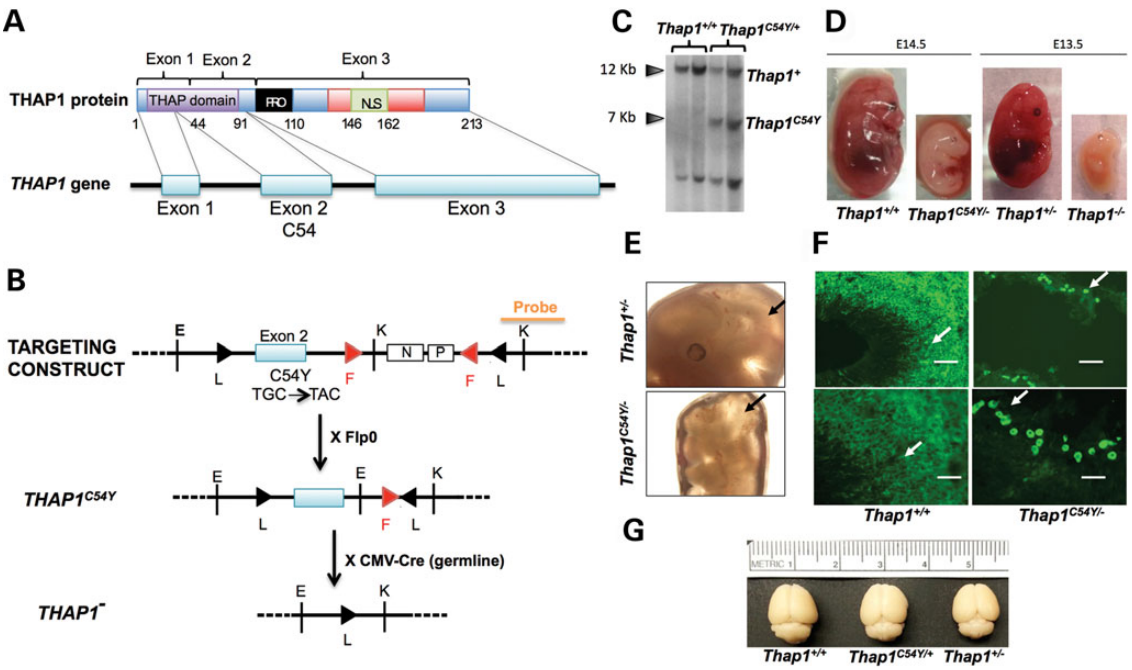

Figure 1. Generation of *Thap1*^{C54Y} and *Thap1*$^{-}$ alleles and mice. (**A**) Schematic representation of *THAP1* gene and Thap1 protein with the THAP domain (purple), low-complexity proline-rich region (black), coiled-coil domain (red) and nuclear localization signal (green). The exon positions are indicated corresponding to the numbers of the amino acid sequence. (**B**) B6;129*Thap1*^{C54YtmLoxPFrt} mutant mouse construct with the inserted LoxP-FRT-PGK-*NeoR*-FRT-loxP cassette. The C54Y mutation is located in Exon 2 flanked by two LoxP sites. The *Thap1*^{C54Y} allele was generated by crossing with the Flp(o) mouse, and subsequently, the *Thap1*$^{-}$ allele was generated by crossing with the CMV-Cre mouse. Green arrows represent the position of the forward and reverse primers used for genotyping. Orange line represents the probe used for Southern blot analysis. E, EcoRV; K, KpnI; F, Frt site; L, LoxP site. (**C**) Southern blot analysis of 10 and 20 µg of KpnI/EcoRV digested genomic DNA from *Thap1*$^{+/+}$ and the B6;129*Thap1*^{C54YtmLoxPFrt} ES clone ultimately used to produce the mice. The *Thap1*$^{+/+}$ sample has bands at 12- and 3-kb bands whereas the positive clone has an additional band at 7.2 kb. (**D**) Representative *Thap1*$^{+/+}$, *Thap1*$^{C54Y/-}$, *Thap1*$^{+/-}$ and *Thap1*$^{-/-}$ embryos at E14.5 or E13.5. Rare, homozygote mutant survivors at this age are small with multiple malformations. (**E**) Transillumination of a *Thap1*$^{+/-}$ skull compared with a *Thap1*$^{C54Y/-}$ skull at E12 shows that the brain is grossly smaller in size, with relatively increased ventricular size (arrows). (**F**) Immunofluorescence with anti-Tuj1 of the cerebral cortex in sections derived from embryos pictured in (**E**) shows a paucity of positively stained neurons and projections in the *Thap1*$^{C54Y+/-}$ brain. The immunopositive 'neurons' are of abnormal shape and size. Regions identified by arrows in upper panels are shown at higher power in lower panels. Scale bars: 50 µm. (**G**) Brains of *Thap1*$^{C54Y/+}$ and *Thap1*$^{+/-}$ mice are of normal size relative to *Thap1*$^{+/+}$, and the exterior is grossly normal.

when suspended by the tail. Weights were similar to littermate controls [$n = 7$–12 for each sex and genotype, *t*-test, $P > 0.05$ for each comparison; male *Thap1*$^{C54Y/+}$: WT 30.9 ± 1.6 (SEM) and *Thap1*$^{C54Y/+}$ 33.4 ± 1.7; female *Thap1*$^{C54Y/+}$: WT 25.7 ± 1.2 and *Thap1*$^{C54Y/+}$ 26.0 ± 0.9; male *Thap1*$^{+/-}$: WT 31.5 ± 1.4 and *Thap1*$^{+/-}$ 30.4 ± 1.0; female *Thap1*$^{+/-}$: WT 26.3 ± 0.8 and *Thap1*$^{+/-}$ 25.8 ± 1.3]. Naïve mice were evaluated in the elevated plus maze to ensure that anxiety-like behavior would not influence performance on motor tasks (Supplementary Material, Figs S2 and S3). There was no significant difference in the time spent in the open and closed arms or in the neutral zone between the *Thap1*$^{C54Y/+}$ or *Thap1*$^{+/+}$ mice of both sexes ($n = 9$ males and $n = 12$ females per genotype) or of the *Thap1*$^{+/-}$ mice of both sexes and their *Thap1*$^{+/+}$ littermates ($n = 8$ per genotype and sex). Both sexes of each recombinant genotype also had normal baseline locomotor activity for 60 min (total, ambulatory and stereotypy; two-way ANOVA, $P > 0.05$) (Supplementary Material, Figs S4 and S5). We performed further motor function assays in the KI and null hemizygous mice of both sexes. Assays included rotarod, gait analysis, beam walking challenge and pole test, with one test carried out each week over consecutive weeks. In all cases, males and females were assigned to a cohort at weaning and tested separately so statistical analysis was performed individually for each sex.

In the accelerating rotarod assay, on testing days, only the female *Thap1*$^{C54Y/+}$ mice displayed a genotype-dependent difference in performance (two-way ANOVA with Bonferroni *post hoc* testing: $F = 4.6$, $Df = 1$, $P < 0.05$) (Fig. 3A). We note, however, that the *t*-test of individual trials was significant ($P < 0.05$) for male trial 5 and female trial 6. *Thap1*$^{+/-}$ male and female mice did not display any abnormality on the rotarod test.

Mice were trained to cross a large beam of 20 mm width for 2 consecutive days with three trials per day and then tested on the medium (10 mm) and narrow (7 mm) beams. We measured latency to cross and foot-slips on 2 testing days with two trials per day. There was no difference in latency to cross between *Thap1*$^{C54Y/+}$ and *Thap1*$^{+/+}$ mice during training, or on the test days. However, the *Thap1*$^{C54Y/+}$ mice had an increase in the number of foot-slips compared with *Thap1*$^{+/+}$ mice. Both *Thap1*$^{C54Y/+}$ sexes showed deficits on the narrow beam on testing Day 1 (unpaired *t*-test, $P < 0.05$ for males and <0.01 for females). Males actually exhibited a worsening performance on the second day of testing on the medium beam relative to *Thap1*$^{+/+}$ ($P < 0.05$) whereas females improved (Fig. 3B). Female *Thap1*$^{+/-}$ mice showed a strong tendency to a 75% increase in foot-slips on the narrow beam on Day 4 ($P = 0.06$).

Gait analysis was manually analyzed (Fig. 3C). There was a decrease in stride length of both paws in *Thap1*$^{C54Y/+}$ males ($P < 0.001$), whereas in females, the hind paw base width was abnormal ($P < 0.01$). The overlap between fore- and hind paws was not significantly different from control in either sex, although males showed a strong trend toward a larger overlap compared with *Thap1*$^{+/+}$ mice (males: $P = 0.052$). Male *Thap1*$^{+/-}$ mice displayed abnormal forepaw stride length and base width ($n = 8$ of each genotype, 5 and 17% increase, respectively, $P < 0.001$).

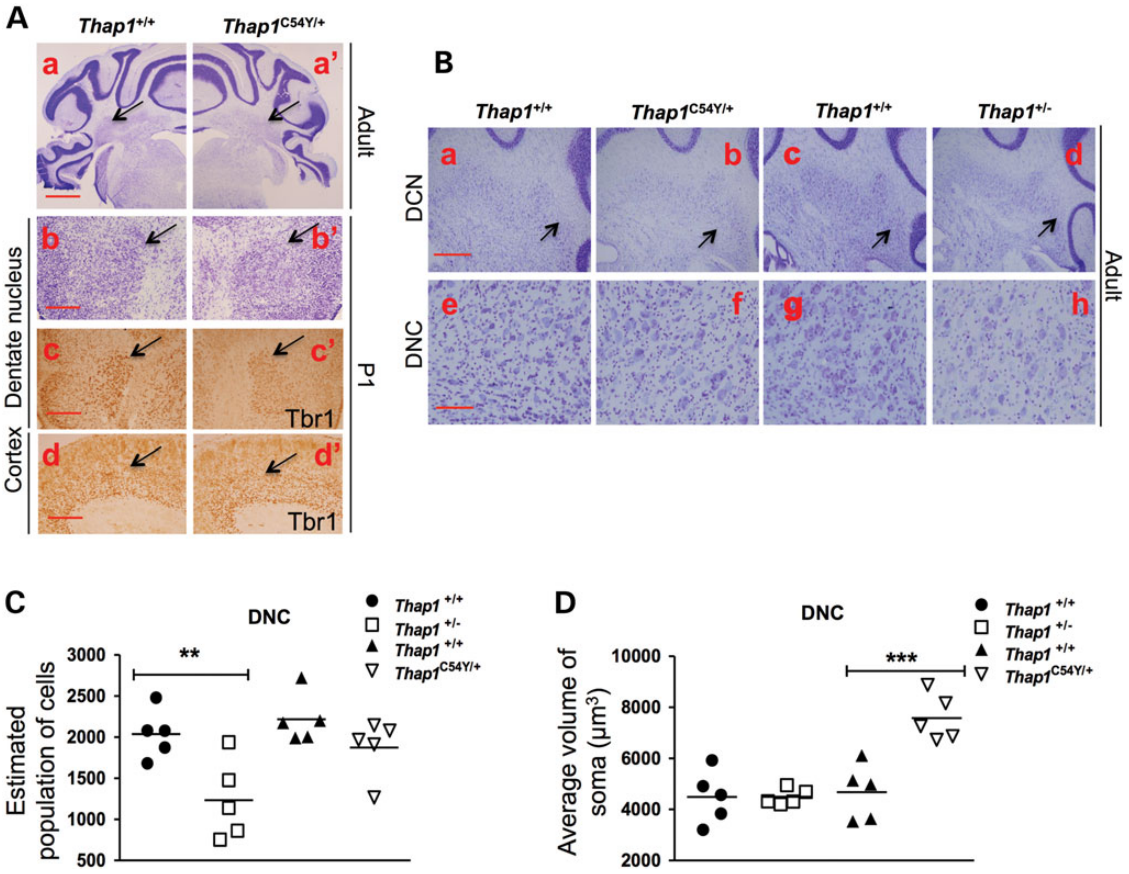

Figure 2. The projection neurons of the DNC are abnormal in *Thap1*$^{C54Y/+}$ and *Thap1*$^{+/-}$ mice. (**A**) Nissl stain of the adult cerebellum (a, a′) shows grossly normal architecture in the adult *Thap1*$^{C54Y/+}$ mouse. Notably, whereas cellularity in the folia appears normal, the deep cerebellar nuclei appear abnormal (arrows, a, a′). The dentate nucleus (arrows) also appears hypocellular at P1 in the *Thap1*$^{C54Y/+}$, as detected with Nissl stain (b, b′) and an anti-Tbr1 antibody (c, c′), a marker of the projection neurons, which appears less intense. Immunostaining with anti-Tbr1 in the cortex of the P1 *Thap1*$^{C54Y/+}$ is similar to the WT (arrows, d, d′). (**B**) Under higher power, Nissl stain of cerebellum shows hypocellularity in the deep nuclei of the cerebellum of the *Thap1*$^{C54Y/+}$ and *Thap*$^{+/-}$ mouse, most prominent in the dentate (lateral) nucleus, indicated by arrows (a–d) and more obvious at higher power (e–h). (**C**) Hypocellularity is confirmed by stereologic counts of large projection neurons in the dentate nucleus of the *Thap*$^{+/-}$ mouse, which reveals a 40% decrease relative to WT ($n = 5$ of each genotype; $^{**}P < 0.01$) and not in the *Thap1*$^{C54Y/+}$ mouse ($n = 5$ of each genotype, $P > 0.05$). (**D**) The large projection neurons in the dentate nucleus of the *Thap1*$^{C54Y/+}$ mouse are of increased volume (Bonferroni's multiple comparison test; $^{***}P < 0.001$), but the large projection neurons in the *Thap*$^{+/-}$ mouse are of normal volume. Note: each genotype had its own set of litter-matched controls for each assay. $^{**}P < 0.01$; $^{***}P < 0.001$. Scale bars: (A) a = 500 µm; b–d = 100 µm. (B) a = 250 µm, e = 100 µm.

Female *Thap1*$^{+/-}$ mice had normal stride length, with a 10% decrease in forepaw base width ($P = 0.045$) and almost a 20% increase in front and hind paw overlap ($P = 0.004$).

In the pole test, we measured time to orient downwards (t-turn) and total time to descend the pole (t-total) (Fig. 3D and E). Male and female *Thap1*$^{C54Y/+}$ mice surprisingly took less time to descend the pole than *Thap1*$^{+/+}$ mice (unpaired t-test, $P < 0.05$) (Fig. 3D). t-Turn times were independent of genotype in *Thap1*$^{C54Y/+}$ mice, although the females displayed a strong trend toward a shorter turn time. Male *Thap1*$^{+/-}$ mice were also faster to orient downwards than their respective controls ($P < 0.05$) (Fig. 3E). In marked contrast, female *Thap1*$^{+/-}$ mice were slower in both orienting downwards and descending than their littermate controls ($P < 0.05$ and 0.01, respectively) (Fig. 3E).

Downstream targets of Thap1 are differentially regulated according to genotype and brain region in heterozygote *Thap1*$^{C54Y/+}$ and *Thap1*$^{+/-}$

It is assumed, albeit unproven, that the pathophysiology of DYT6 includes transcriptional dysregulation, and studies to date in peripheral cells imply that there are overlapping as well as cell-specific differences in downstream regulation (7,8). Therefore, we first used a targeted approach to examine gene expression in the recombinant mice in striatal and cerebellar mRNA derived from mice at ages P1 and 2.5 months to determine whether there were age and regional differences, using published results as a guide.

The first gene of interest was *Thap1* itself, and mouse (m) and human (h) *Thap1* mRNAs were measured by quantitative real-time PCR using TaqMan assays, which we documented to be species specific. This assay amplified across the Exon 2–3 junction, and Exon 2 is deleted in the null allele. In the adult *Thap1*$^{C54Y/+}$ mouse, m*Thap1* was unchanged in the striatum but was increased in the cerebellum (+42%, $P < 0.001$) [Table 1(B)] and testis (+15%, $P < 0.001$), in which Thap1 is expressed in greater abundance than that in the brain (20). At P1, *mThap1* was increased in both striatum (+31%, $P < 0.01$) and cerebellum (+43%, $P < 0.05$) (Table 1). On the other hand, *Thap1*$^{+/-}$ heterozygote mice displayed a 50% decrease of *mThap1* mRNA in the striatum and cerebellum at both P1 and adult (Table 1).

We then sought to determine whether Thap1 protein and mRNA levels correlate. We have shown that in neuronal

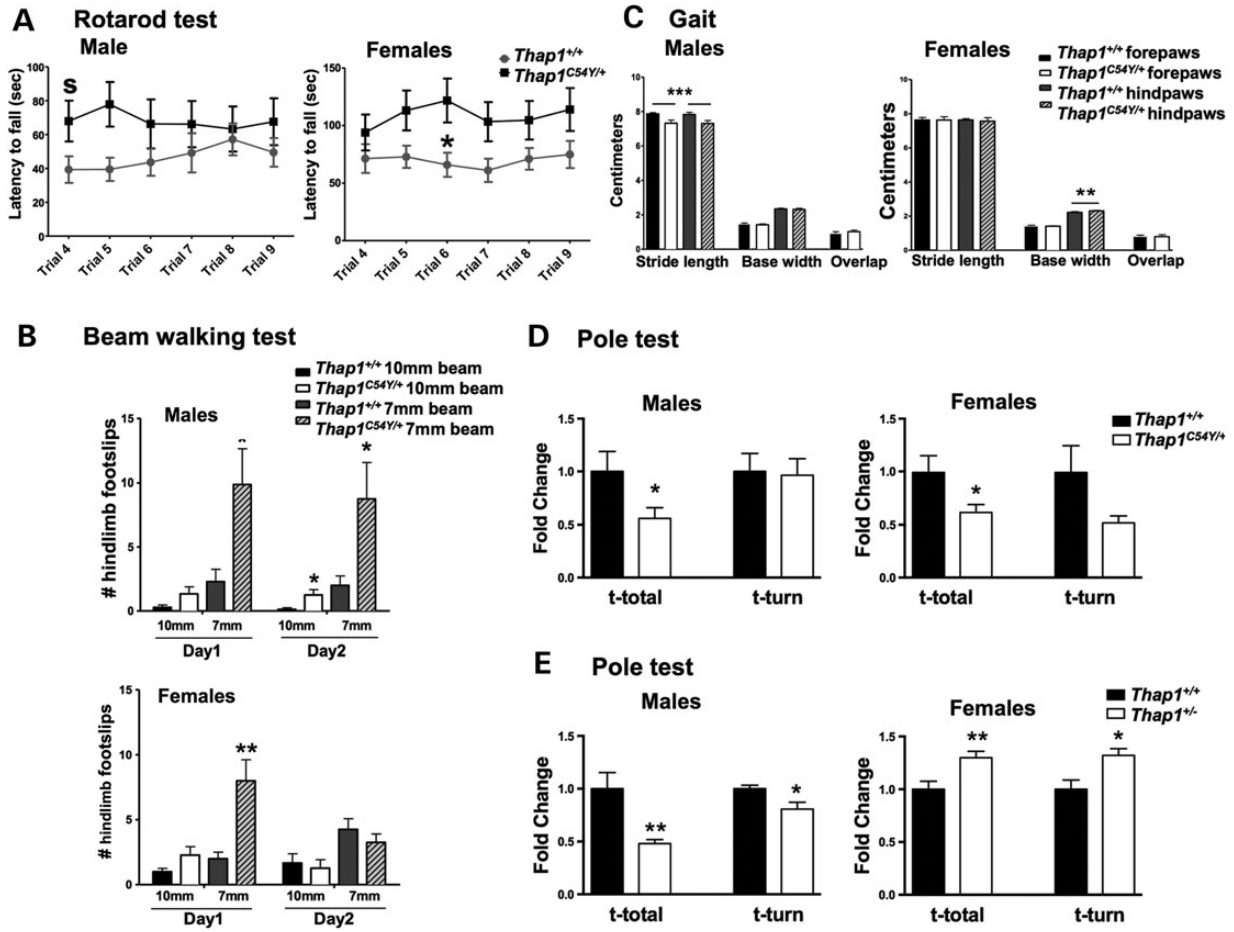

Figure 3. *Thap1*$^{C54Y/+}$ and *Thap1*$^{+/-}$ mice display abnormalities of motor function. (**A**) On the accelerating rotarod testing days, the female *Thap1*$^{C54Y/+}$ performance was significantly worse compared with their *Thap1*$^{+/+}$ littermates (error bars indicate SEM; two-way ANOVA followed by Bonferroni *post hoc* test) ($n = 9$ males and $n = 12$ females for all assays). (**B**) On the beam walking test days, male and female *Thap1*$^{C54Y/+}$ mice exhibited an increased number of foot-slips on the first test day on the small 7 mm beam compared with their *Thap1*$^{+/+}$ littermates (unpaired *t*-test, $P < 0.05$). Males were not able to learn, showing a worse performance also on the second day of testing ($P < 0.05$). (**C**) In the gait analysis, *Thap1*$^{C54Y/+}$ males showed a decrease in stride length and the females had a wider base width of the hind paws compared with *Thap1*$^{+/+}$ (*t*-test: stride length males: $P < 0.001$; females: $P > 0.05$ and base width males: $P > 0.05$; females: $P < 0.01$; overlap: n.s.). (**D**) On the pole test, *Thap1*$^{C54Y/+}$ male and female mice displayed a lower total time to descend the pole, i.e. descended faster, compared with *Thap1*$^{+/+}$ in both sexes (unpaired *t*-test: $P < 0.05$). (**E**) *Thap1*$^{+/-}$ males also displayed a lower total time to descend the pole compared with *Thap1*$^{+/+}$ ($n = 6$; $P < 0.01$) and also decreased *t*-turn time ($P < 0.01$). In contrast, *Thap1*$^{+/-}$ females ($n = 8$) were slower to orient downwards ($P < 0.05$) and to descend ($P < 0.01$), i.e. greater *t*-turn and *t*-total. $^{*}P < 0.05$; $^{**}P < 0.01$.

Table 1. Regulation of downstream targets of Thap1 in the brain is genotype, age and region dependent

Gene ID	*Thap1*$^{C54Y/+}$				*Thap1*$^{+/-}$			
	P1	Mean ± SEM	Adult	Mean ± SEM	P1	Mean ± SEM	Adult	Mean ± SEM
(A) Striatum								
mThap1	(+) 31%**	131.4 ± 7.0	ns	112.3	(–) 49%*	50.9 ± 8.7	(–) 50%***	50.1 ± 2.1
rrm1	(+) 28%*	128.4 ± 8.1	ns	102 ± 5.2	ns	84.9 ± 27.3	ns	101.8 ± 1.4
Tor1A	ns	113.9 ± 26.1	ns	106 ± 10.9	ns	77.9 ± 8.2	nd	nd
Slc6a13	(+) 210%*	239.8 ± 57.6	(+) 47%*	147 ± 13.4	ns	16.9 ± 4.7	ns	79.0 ± 5.8
(B) Cerebellum								
mThap1	(+) 43%*	143 ± 9.3	(+) 42%***	142.2 ± 4.3	(–) 53%***	47.0 ± 5.8	(–) 43%**	57.5 ± 6.2
rrm1	ns	91.2 ± 6.4	ns	97.1 ± 7.8	ns	95.8 ± 3.9	ns	90.9 ± 7.4
Tor1A	ns	111.6 ± 10.3	ns	87.9 ± 8.6	nd	nd	nd	nd
Slc6a13	nd	nd	ns	137 ± 16.8	nd	nd	nd	nd

Quantitative real-time PCR analyses showing mRNA expression levels in the striatum (A) and cerebellum (B) of the *Thap1*$^{C54Y/+}$ and *Thap1*$^{+/-}$ mice. Results are expressed as percentage relative to *Thap1*$^{+/+}$. Unpaired *t*-tests were conducted between genotypes: $^{*}P < 0.05$; $^{**}P < 0.01$; $^{***}P < 0.001$. P1: postnatal day 1; $n = 4$–8.
ns, not significant; nd, not done; P1, postnatal day 1.

structures, mThap1 appears as 30–32 and 50-kDa bands, both frequently doublets, and the latter being neuronal specific, localized to the nucleus and capable of binding DNA. Using homozygous-null tissue from embryos, we also demonstrated that the 50-kDa band recognized by the ProteinTech antibody used in the current study is overwhelmingly authentic Thap1, but that the 30-kDa band contains a large amount of a cross-reacting protein. Finally, we showed that in the heterozygote-null embryo, the level of the 50-kDa isoform was similar to that of the WT (20). For this study, therefore, we quantitated only the 50-kDa band. In the striatum of the *Thap1*$^{+/-}$ mouse, the level of the 50-kDa Thap1 protein was decreased at 2 months of age but normalized by 3 months (Fig. 4A). In the adult *Thap1*$^{C54Y/+}$ mouse, the level of the 50-kDa isoform was similar to WT in striatum (Fig. 4A), whole brain and cerebellum (Supplementary Material, Fig. S6), the latter despite a significant increase in mRNA, but as discussed below, these data must be interpreted with caution.

RRM1 is a documented target of Thap1 in endothelial cells (7). It encodes a ubiquitously expressed subunit of ribonucleoside-diphosphate reductase most active during the S-phase of mitosis and regulated by pRB-E2F (21). *Rrm1* mRNA was up-regulated in P1 *Thap*$^{C54Y/+}$ striatum, whereas its level was unchanged in both regions of adult mice of both recombinant genotypes (Table 1). *Dnmt1* is associated with developmental and adult neuronal function and neuropsychiatric disorders (22) and is another purported target of Thap1 in HUVECs (7), but *Dnmt1* mRNA was unaltered in any of the P1 or adult samples in which it was assayed.

Much evidence supports the notion that disruption of catecholamine signaling, particularly dopamine, contributes to the pathophysiology of early onset torsion dystonia. We screened expression of genes involved in G-protein-coupled receptor (GPCR) function by microarray (SABiosciences, ARRAY #PAMM-071Z) in the striatum of adult *Thap1*$^{C54Y/+}$ mice ($n = 4$). Of the genes included in this array, all were unchanged except *Lpar1*, *Ccl2*, *Ccl4* and only the latter with a change of at least 2-fold. We were unable to validate any of these changes by real-time quantitative polymerase chain reaction (RT-qPCR). Genes assayed in this commercial microarray include *Drd1*, *Drd2*, *Acy5*, *Rgs2*, *Adora2a* and multiple genes implicated in striatal synaptic plasticity, e.g. *Egr1*, *Fos*, *Jun* and *JunB*. We assayed additional potentially relevant genes in these same pathways, and *Rgs9*, *Rgs14*, *Pde10a* and *Egr3* mRNAs were all unchanged, as were protein levels of tyrosine hydroxylase (TH), Gαolf (causative gene for DYT25) (1) and DARPP-32 (Fig. 4B and C).

Additionally, we looked for genes included in the GPCR array that were abnormal in lymphoblastoid lines from a DYT6 patient (c.71+9C>A sequence variant) (8). There were four genes, *Bai1*, *Elk4*, *Agt* and *Mmp9*, that were dysregulated in the lymphoblastoid

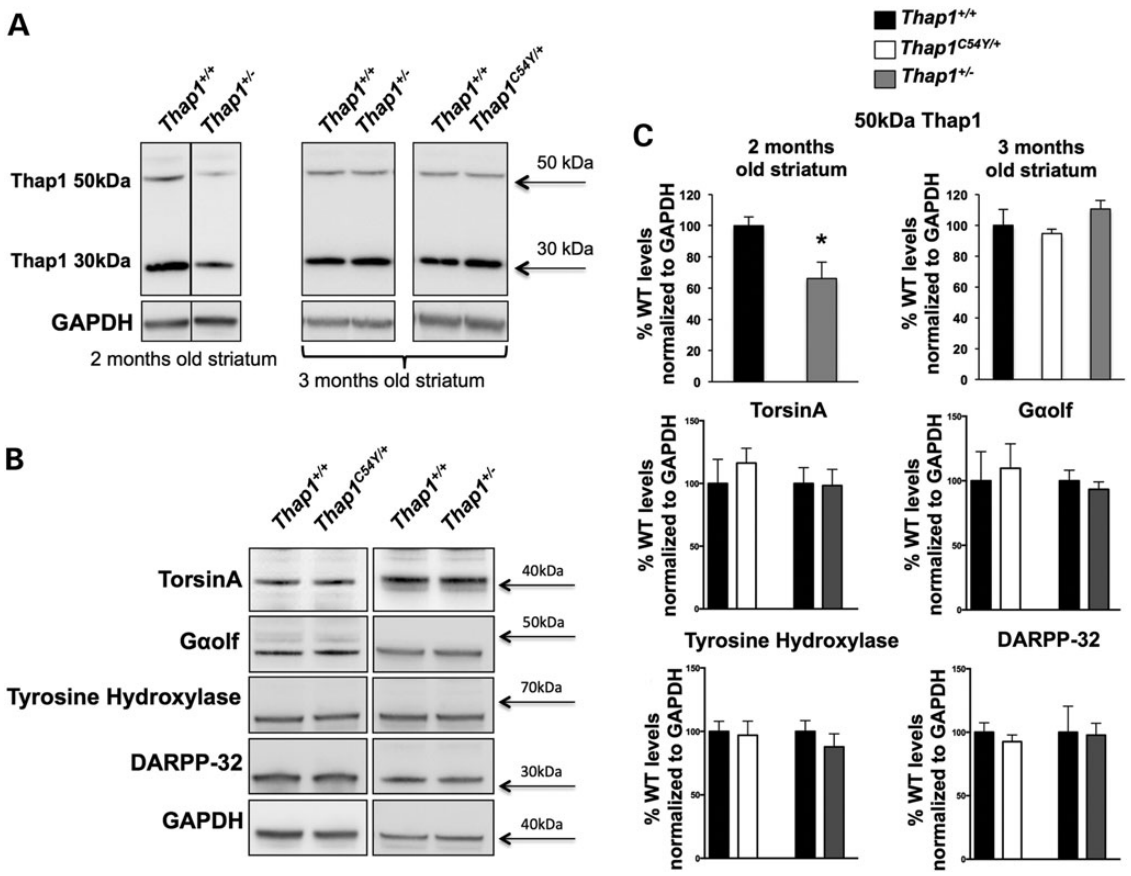

Figure 4. Protein levels of torsinA, Gαolf, DARPP-32 and TH are unchanged in *Thap1*$^{C54Y/+}$ and *Thap1* $^{+/-}$ mice. (**A**) Western blot analysis of Thap1 in 30 μg of striatal total cellular homogenates showed a significant decrease of the 50-kDa isoform at 2 months of age in *Thap1*$^{+/-}$ mice but no difference at 3 months of age, at which time it was also unchanged in *Thap1*$^{C54Y/+}$ mice relative to *Thap1*$^{+/+}$. GAPDH is displayed as a loading control. Blots are representative of $n = 3$ per genotype for *Thap1*$^{C54Y/+}$ and $n = 5$ per genotype for *Thap1*$^{+/-}$ mice. Densitometry values were normalized to GAPDH, and Thap1$^{+/+}$ levels were set arbitrarily at 100%. (**B**) Western blot analysis of total cellular homogenates from adult Thap1$^{C54Y/+}$ and Thap1$^{+/-}$ striatum (20 μg protein per lane). Baseline levels of TH, DARPP-32, Gαolf and TorsinA are similar in the two recombinant mice compared with their Thap1$^{+/+}$ littermates. GAPDH is displayed as loading control. $n = 4$ per genotype. (**C**) Densitometry values were normalized to GAPDH and Thap1$^{+/+}$ levels were set arbitrarily at 100%. $P > 0.05$ (unpaired two-tailed t-test).

lines but not in the *Thap1*$^{C54Y/+}$ striatum. Finally, we chose several genes for RT-qPCR from the lymphoblastoid array, which are expressed in the brain. Most relevant to this report, the GABA transporter *Slc6a13* was down-regulated in lymphoblastoid mutant lines but, in the mice characterized herein, was up-regulated in a genotype-, age- and region-dependent fashion (Table 1).

Tor1a mRNA and torsinA protein levels are unchanged in *Thap1*$^{C54Y/+}$ and *Thap1*$^{+/-}$ mice

Tor1a mRNA and/or protein levels were measured in all three genotypes based on the reports of interaction and regulation of the DYT1 TOR1A gene by Thap1 *in vitro* (14,15). In the two recombinant mice described herein, *Thap*$^{C54Y/+}$ and *Thap*$^{+/-}$, there were no differences in *Tor1a* mRNA (Table 1) or torsinA protein levels in striatum or cerebellum at P1 and in the adult (Fig. 4B and C).

Noradrenaline level in the *Thap1*$^{C54Y/+}$ and *Thap1*$^{+/-}$ striatum is increased and response to d-amphetamine plus propranolol is altered in the THAP1$^{C54Y/+}$ mouse

To measure monoamines and their metabolites, striatum and cerebellum were analyzed by HPLC in the Neurochemistry Core at Vanderbilt University Medical Center (Nashville, TN). The levels of striatal and cerebellar serotonin and dopamine, and their metabolites and ratios (Table 2) in *Thap1*$^{C54Y/+}$ mice and in the striatum of *Thap1*$^{+/-}$ mice were equal to WT littermates. Noradrenaline (NA) was increased in the striatum of *Thap1*$^{C54Y/+}$ and *Thap1*$^{+/-}$ mice when analyzed by individual *t*-tests, but by one-way ANOVA with Bonferroni's multiple comparison, *P*-values were not significant.

Striatal NA level is very low, so even though significant by *t*-test, we interpreted these data with caution. Although TH protein level is normal in the striatum, only a small percentage of TH-immunopositive projections in the striatum are derived from the locus coeruleus (LC). Immunostaining for TH in the LC of *Thap1*$^{C54Y/+}$ mouse appeared grossly normal (Supplementary Material, Fig. S1B). Therefore, to initiate a functional assay of the striatal dopamine and NA systems, we assayed the response to D-amphetamine and the nonselective β-adrenergic antagonist propranolol, which enhances the locomotor response to d-amphetamine in WT mice (23). Male and female *Thap1*$^{+/+}$ and *Thap1*$^{C54Y/+}$ were injected intraperitoneally with either 20 mg/kg of (S)-(−)-propranolol hydrochloride or an equal volume of saline, and after 30 min, all mice were injected with 2 mg/kg of d-amphetamine. Total activity was recorded, as were its ambulatory and stereotypy components, for 30 min after propranolol and 45 min after amphetamine (Fig. 5). In the male control cohort (Fig. 5A), there was a significant interaction between time and propranolol (two-way RM ANOVA: $F = 1.98$, $P = 0.03$), which was not present in the KI group ($F = 0.27$, $P = 0.99$). Although the interaction was significant only when analyzing the total locomotor activity, the major genotype-dependent difference was in stereotypical activity following amphetamine. However, no single point in time was significant on the *post hoc* test for any of the three measurements. The same assay in females (Fig. 5B) resulted in an interaction between time and genotype for total locomotor activity (interaction $P = 0.007$, $Df = 8$, $F = 2.84$; genotype, $P = 0.01$, $Df = 1$, $F = 7.99$; Bonferroni *post hoc* text, $P < 0.05$ at 25 and 40 min), indicating an increased response to amphetamine in the KI mouse in the absence of propranolol. The WT female mice exhibited an enhanced response to amphetamine following propranolol (Fig. 5B; at 35 min, Bonferroni *post hoc* test, Diff = 114.9, $t = 2.96$, $P < 0.05$), whereas the KI females failed to show this induction. These data suggest that the KI mice are more sensitive to the ambulatory effects of a low dose of amphetamine. Moreover, the failure of propranolol to amplify this response, as it does in the WT, implies a lower reliance on production of cAMP via the β-adrenergic receptor in the KI mice (23).

Table 2. Noradrenaline is increased in the striatum of *Thap1*$^{C54Y/+}$ and *Thap1*$^{+/-}$ mice

HPLC Striatum	Thap1$^{C54Y/+}$ ($n = 5$) Mean (%) ± SEM	*P*-value	Thap1$^{+/-}$ ($n = 4$) Mean (%) ± SEM	*P*-value
DOPAC	115.8 ± 6.3	ns	116.1 ± 6.8	ns
DA	95.8 ± 4.5	ns	102.5 ± 4.6	ns
HVA	97.9 ± 2.6	ns	114.2 ± 9.8	ns
DOPAC/DA	122.6 ± 10.6	ns	112.2 ± 3.2	ns
HVA/DA	102.6 ± 3.8	ns	108.6 ± 8.4	ns
3-MT	100.5 ± 6.5	ns	115.6 ± 3.5	ns
5-HIAA	107.6 ± 1.5	ns	110.4 ± 7.8	ns
5-HT	104.0 ± 3.6	ns	114.1 ± 8.2	ns
NA	152.9 ± 9.4	<0.01**	143.6 ± 12.5	<0.05*

Quantitative HPLC analysis of the biogenic monoamines in *Thap1*$^{C54Y/+}$ and *Thap1*$^{+/-}$ striatum. Results are expressed as average ng/mg tissue ± SEM ($n = 5$) and normalized to *Thap1*$^{+/+}$, arbitrarily set at 100%. Unpaired *t*-test, *P < 0.05; **P < 0.01.

Discussion

We generated and characterized the first mice harboring genetic abnormalities of the DYT6 gene, *Thap1*, including a KI C54Y allele and a *Thap1* null allele. We sought to determine whether these mice display motor or molecular phenotypes consistent with some of the major proposed causes of human primary dystonias and comparable to other mouse models of genetic dystonia. In comparing this panel of mice against humans with DYT6, it is notable that none of these recombinant mice displayed any spontaneous movement disorder, similar to human NMCs. These data imply either that the presence of a single WT *Thap1* allele in the mouse is sufficient to prevent overt disease and/or that there are naturally occurring compensatory or suppressor mechanisms. Both genotypes, however, displayed abnormalities that can be ascribed to neural systems associated with dystonia. Our data thereby provide important leads as to how dysfunction of Thap1 might result in the human DYT6 phenotype.

Neuronal molecular consequences of a mutant or null *Thap1* allele are both shared and genotype-unique. In addition, within the brain, the abnormalities are age and region dependent. Both the KI and null alleles are early embryonic lethal in the homozygote state, and importantly, *Thap1*^{C54Y} is unable to rescue the *Thap1* null embryo. Demise at these ages raises the possibility of placental dysfunction in addition to organ abnormalities. These data imply a loss-of-function, yet there are DYT6 patients homozygous for mutant *THAP1* (24), so these data are consistent with the theory that *THAP1* mutations may vary in their level of disruption of Thap1 function.

Morphology

The most robust abnormalities described herein are in the projection neurons of the DNC. Mice lacking brain torsinA develop spontaneous twisting movements with gliosis and apoptosis in sensorimotor regions, including the deep cerebellar nuclei (13). Although non-physiologic relative to the DYT1 genotype, those data serve to highlight brain regions that developmentally require torsinA. Subtle microstructural changes exist in the

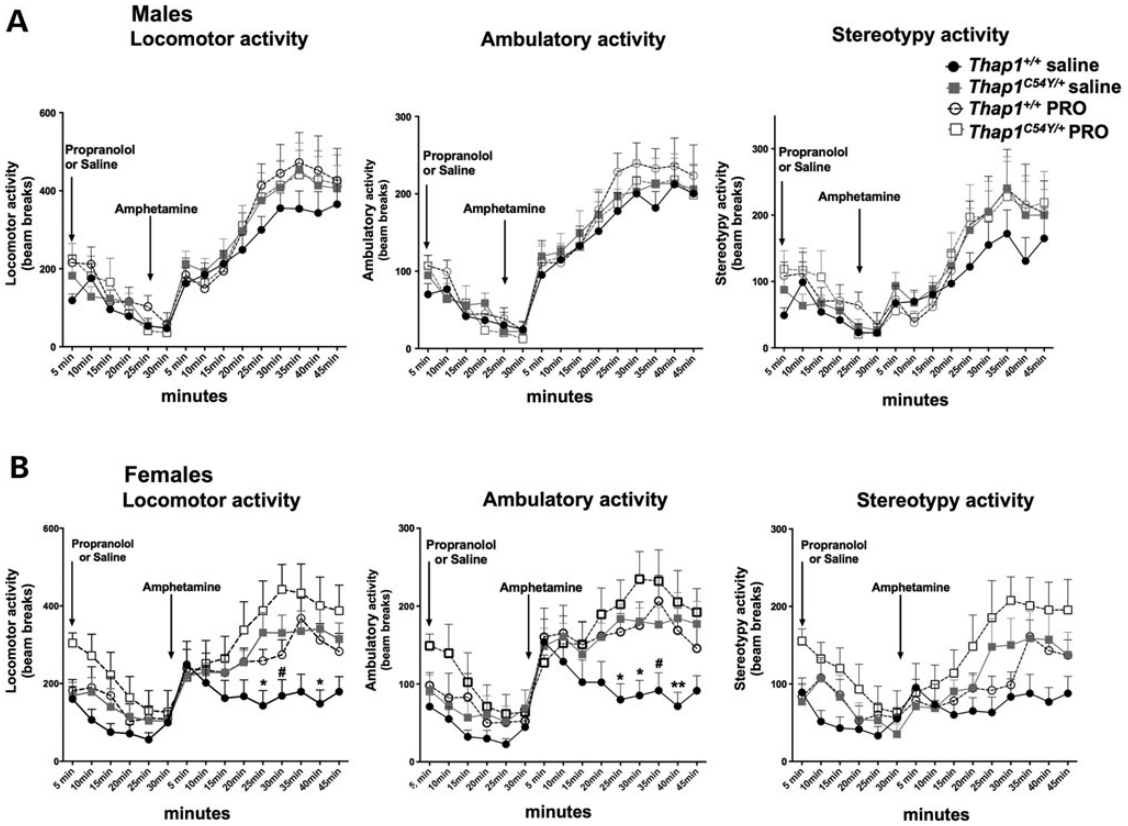

Figure 5. *Thap1*$^{C54Y/+}$ mice display altered response to injection of the β-adrenergic antagonist propranolol followed by d-amphetamine. (**A**) Locomotor, ambulatory and stereotypy activities of *Thap1*$^{C54Y/+}$ male mice following administration of d-amphetamine (i.p., 2 mg/kg) after the nonselective β-adrenergic antagonist (S)-(−)-propranolol injection (PRO) (i.p., 20 mg/kg) or saline (2-month-old males: $n = 8$ of each genotype per treatment). Locomotion was quantified for 30 min after saline or propranolol injections and 45 min after amphetamine injection. Mice were habituated to the cages for 15 min prior to the first injection. There was a significant interaction between saline and propranolol groups in the *Thap1*$^{+/+}$ (two-way ANOVA), but individual time points were not significant with Bonferroni *post hoc* test. Data points represent mean activity ± SEM. (**B**) *Thap1*$^{C54Y/+}$ female mice and littermate controls ($n = 8$) were treated similarly to males in (A). Genotype-dependent differences were noted in locomotor or ambulatory activity following amphetamine in the absence of propranolol, indicating an increased response of the recombinant mice to amphetamine but a relatively lower contribution of NA activity to cAMP production following the psychostimulant. In the locomotor activity panel, asterisk represents *Thap1*$^{+/+}$ saline/amphetamine versus *Thap1*$^{C54Y/+}$ saline/amphetamine and hash represents *Thap1*$^{+/+}$ saline/amphetamine versus *Thap1*$^{+/+}$ propranolol/amphetamine. In the ambulatory panel, asterisk represents *Thap1*$^{+/+}$ saline/amphetamine versus *Thap1*$^{C54Y/+}$ saline/amphetamine and hash represents *Thap1*$^{+/+}$ saline/amphetamine versus *Thap1*$^{+/+}$ propranolol/amphetamine (Bonferroni *post hoc* test * or $^{\#}P < 0.05$; $^{**}P < 0.01$).

cerebellum of DYT1 KI mice (25,26). The marked decrease in large projection neurons in the DNC in the 'physiological' *Thap1*$^{+/-}$ mice and increased soma size in the *Thap1*$^{C54Y/+}$ mice strongly support the notion of an underlying abnormality of this structure in more than one form of primary dystonia. Hypocellularity of the DNC might result in decreased cerebellar output, consistent with brain imaging in DYT1 and DYT6 patients (2). Neuronal hypertrophy, most studied owing to PTEN/PI3K/Akt/mTORC(1 or 2) pathway mutations (27), has profound effects on plasticity, which is disordered in dystonia. Of note, the PI3K signaling pathway was among the most perturbed in the reported microarray from DYT6 patient lymphoblasts (8).

Transcription

Knockdown or overexpression of Thap1 in HUVECs reportedly led to a similar phenotype owing to down-regulation of mRNA levels of *THAP1* itself (7). The authors concluded that overexpression of Thap1 represses function of endogenous Thap1 and that cell viability requires regulation of Thap1 level within a narrow range. A recent report from a second group confirmed the *THAP1* mRNA auto-regulatory phenomenon (9). In corroboration of those reports, we found that *Thap1* mRNA was increased *in vivo* in the presence of the KI C54Y mutation but we show for the first time that transcriptional dysregulation in Thap1-recombinant mice is neuronal subtype and age dependent. Transcriptional alterations vary between striatum and cerebellum and are generally greater at younger ages, consistent with a developmental component of the disease. Although we were unable to demonstrate a corresponding increase in level of the 50-kDa isoform in *Thap1*$^{C54Y/+}$ mice, we would not yet conclude that Thap1 protein is never increased, for both technical and physiologic reasons. The antibodies available preclude quantification of the lower-molecular-weight form of the protein, and it is also possible that the mutant allele is over-transcribed but the resultant protein is less stable than the WT (9). In the presence of a null allele, *Thap1* mRNA was decreased by 50%, but the level of the 50-kDa Thap1 protein isoform in the striatum varied with age, consistent with post-transcriptional regulation as seen in other heterozygote-null mice with phenotypes (28,29). Auto-regulation thus appears to occur on several levels. Albeit speculative, we also hypothesize that behavioral and cellular abnormalities that are observed despite sometimes apparently normal level of the Thap1 50-kDa isoforms in the hemizygous-null mouse are most likely due to cell type- or age-specific differences and/or the sensitivity of certain Thap1 bioactivities to very small changes in protein level of any

of the multiple Thap1 forms (10), for which precedents exist in hemizygous-null mutant mice (e.g. 29).

Microarray data from HUVECs with altered Thap1 levels identified changes in levels of only 86 genes, which were enriched for cell cycle control genes (7). Dysregulation of cell cycle genes plays a role in many neuropsychiatric diseases (30). Notably, *Rrm1* mRNA level was altered in the P1 *Thap1*$^{C54Y/+}$ striatum. A preliminary survey of the homozygote-null and -*Thap1*^{C54Y} embryos, along with decreased neuronal number in the DNC of heterozygotes, suggests that dysregulation of neurogenesis, apoptosis and/or differentiation may be occurring. Thus, a full picture of transcriptional dysregulation by *THAP1* mutations will require genome-wide approaches in the presence of different mutations, and surveys of multiple brain regions and cell subtypes from animals of all ages.

Catecholamines

Mice with a KI or null allele both appeared to display an increase in striatal NA. The dopamine system has received the most attention in dystonia studies (31,32), particularly with the identification of *GCH1* mutations causing dopa-responsive dystonia (33) and mutations in *GNAL*/$G_{\alpha olf}$ as the cause of DYT25 (32). However, both the DA and NA systems contribute to the pathophysiology of Parkinson's disease and levodopa (L-DOPA)-induced dyskinesia. Our data in the propranolol/amphetamine assay are consistent with abnormalities in both pathways.

Despite sparse NA innervation, striatal medium spiny neurons express a large number of adrenoreceptors (34). Adrenergic receptors are GPCRs, and noradrenergic signals in the striatum are transduced at least in part, via $G\alpha_{olf}$ (35), and may increase or decrease dyskinetic movements. In at least one study, either ablation of LC neurons or genetic deletion of dopamine-β-hydroxylase (DBH) potentiated the motor deficits in animals with dopaminergic lesions. Further, the motor function following deletion of DBH was improved by intracranial NA or paradoxically, with systemic propranolol (36,37). In this study, the superior performance of some of the recombinant mice on the pole test compared with WT mice suggests the presence of up-regulated DA neurotransmission (38), along with the increased ambulatory response of the KI mice to a low dose of amphetamine.

Comparison of *Thap1*-related mice with DYT1 mice

Comparison of the phenotypes of DYT1 and DYT6 mice yields some interesting similarities, including morphologic abnormalities in the deep cerebellar nuclei. Like *Tor1aΔGAG* KI and heterozygote *Tor1a*-null mice (39), the *Thap1*-related mice described herein do not demonstrate abnormal, spontaneous movements. The DYT1 mice demonstrate abnormalities in motor learning and individual motor tasks, particularly beam walking (39). The *Thap1*-related mice demonstrate abnormalities in multiple motor tasks, supporting a role for Thap1 in the regulation of motor function. The abnormalities in gait might best be described as having some elements of ataxia, perhaps arising from the changes in number or morphology of the projection neurons in deep cerebellar nuclei, and there are instances of overlapping ataxia and dystonia in patients and in mouse models. Motor abnormalities might also arise from abnormalities within the catecholamine system present in both DYT6 and DTY1 mice (40–42).

Attempts to mechanistically link forms of early onset torsion dystonia have led to demonstrations of association between Thap1 and the *Tor1a* promoter *in vivo* in mouse brain and regulation of *Tor1a* by Thap1 *in vitro*, but not in DYT6 patient-derived fibroblasts (9,14,15). From this first analysis of effects of a *Thap1* mutation on the regulation of *Tor1a* in neurons, we conclude that in the mouse, a null allele or the expression of Thap1^{C54Y} does not alter the level of *Tor1a* mRNA or torsinA protein. We cannot exclude the possibility that a Thap1/*Tor1a* regulatory interaction is manifested under other conditions or in other tissues.

Finally, the DYT6 recombinant mice described herein displayed sex differences on several motor assays. Several adult onset forms of focal dystonia vary in their sex bias, with some more prevalent in males and others in females (43). There was a report prior to the identification of many of the dystonia genes other than DYT1, which indicated a higher incidence in females for isolated, genetic dystonia (44). There is no evidence among *THAP1* mutation-positive patients for a gender bias, and as most mutations are private, there will likely not be enough power to demonstrate a gender affect for any particular mutation.

Summary

This is the first characterization of neurons and mice harboring a naturally occurring pathogenic human *THAP1* mutation. These data highlight abnormalities in systems and function already associated with dystonia, and age-, cell- and context-specific downstream effects of a *Thap1* point mutation or null allele, indicating the need to study the effects of multiple *THAP1* mutations at different ages and in multiple tissue and neuronal types. Our data are consistent with a role for Thap1 in motor control and suggest that the function of several widely distributed brain regions may be altered in DYT6. In particular, higher brain regions such as those underlying sensorimotor function may be dysfunctional in concert with abnormalities attributable to the noradrenergic system originating in the LC of the brainstem. Finally, disruption of Thap1 functions unrelated to its role in transcription may underlie its embryonic lethality in mice and its pathogenicity in humans. Future studies will focus on refining our characterization of the structural and functional disturbances that are caused by *Thap1* manipulations, in order to elucidate the pathogenesis of DYT6 dystonia.

Material and Methods

Experimental procedures were carried out in compliance with the United States Public Health Service's Policy on Humane Care and Use of Experimental Animals and were approved by the Institutional Animal Care and Use Committee at Icahn School of Medicine at Mount Sinai.

Generation of gene-targeted mice

A targeting construct was created with two LoxP sites flanking Exon 2 with a PGK-Neo cassette flanked by two FRT sites: LoxP-FRT-PGK-*Neo*R-FRT-LoxP via Red/ET recombination (GeneBridges, Heidelberg, Germany). Following electroporation, 129/Sv ES clones with homologous recombination were identified by long-range PCR with two primer pairs: forward: 5′ AGGTTT CCTCTTACTCGCCCCAGCCT 3′ (5′ end of Exon 2), reverse: 5′ CAA GGTTCAAATCTGTTAAAGGA 3′ (3′ of the vector); and forward: 5′ GCACGAGACTAGTGAGACGTGCTAC 3′ (located in antibiotic resistance cassette), reverse: 5′ CAGAAAGCCTGTTTCCCTTCAGT 3′ (5′ to the 3′ end of the vector).

Following microinjection into C57BL/6J blastocysts in the core facility of Icahn School of Medicine at Mount Sinai, males

(B6;129Thap1-C54Y^{tmLoxPFrt}) that were >50% chimeric were crossed with C57BL/6J females, and mutant mice subsequently identified by Southern blot analysis. Genomic DNA was digested with EcoRV and KpnI and Southern blot performed (17). Mice from a single chimera were crossed with Flp(o) mice (45). WT, KI and null alleles were identified by PCR on genomic tail DNA (REDExtract-N-Amp Tissue PCR kit; Sigma, St Louis, MO): forward 5′ GCGTATAATTCAGGCTGTCAG 3′; reverse 5′ GCATTCACCCAA AGCCAATGC 3′ (WT, 779 bp; KI 913 bp; null 254 bp).

Mice with targeted gene mutations were mixed B6;129 background backcrossed three to four generations with C57BL/6J and were 85% C57BL/6J (DartMouse, http://dartmouse.org/).

Behavior

Most assays were performed in mice at 7–9 months of age with investigators blinded to genotype. Assays were performed as previously described, including elevated plus maze (46), locomotor activity (40), (MicroMax Animal Activity Monitors, Digiscan D Microsystem, Columbus Instruments, Columbus, OH), gait analysis (47), pole test (48), rotarod (47) and beam walking (40). Prior to drug administration, mice were habituated to intraperitonial saline injections and the locomotor boxes for three consecutive days. On Day 4, after 15 min in the locomotor box, mice received (*S*)-(−)-propranolol (Sigma) (20 mg/kg ip) or an equivalent volume of saline. Activity was recorded for an additional 30 min, after which all mice received d-amphetamine (2 mg/kg ip).

Real-time polymerase chain reaction

RT-qPCR was performed as previously described (20) using the following Taqman assays: Mm01212603_m1 and Hs00216494_m1 to detect mouse and human Thap1, respectively, Mm00485870_m1 for mouse Rrm1 (ribonucleotide reductase M1), Mm00520052_m1 for Tor1A [torsin family 1, member A (torsin A)], Mm01151063_m1 for TBP (TATA-binding protein), Mm00446968_m1 for HPRT1, Mm02601777_g1 RPS18.

Western blotting

Western blots were performed as previously described (20) using the following antibodies: Thap1 (1:1000; Proteintech); TorsinA (1:500; Abcam Ab34540); TH (1:1000; Chemicon Ab152), DARPP-32 (dopamine and cyclic-AMP-regulated phosphoprotein, 32 kDa) (1:1000; Cell Signaling #2306); GAPDH (1:1000, Santa Cruz sc32233).

Histology and immunocytochemistry

Nissl stain and immunocytochemistry were performed as previously described (47). We used the following antibodies: DARPP-32 (1:1000; Cell Signaling #2306), TH (1:1000; Chemicon Ab152), Tbr1 (1:1000; Abcam ab31940), MOR (1:1000; Immunostar 24216).

Stereology

The DNC was delineated on every section (49), and drawings of the DNC were obtained using the StereoInvestigator software v.10 (MBF Bioscience, Williston, VT) on a Zeiss Axiophot microscope at a 20× magnification. The section thickness was measured with the aid of a microcator at several locations within the region of interest and was found to be 10 ± 3 µm in both genotypes. Our systematic-random design generated 13–29 different locations, in the sampling grid, depending on the section, using 115 × 115 × 7 µm^2 disectors (19,49,50). The average volume of the neuronal somata was estimated with the vertical Nucleator probe in StereoInvestigator using four rays and assessed 150–300 neurons depending on the animal, yielding individual coefficient of errors of <10%. From this sampling, the total number of large neurons (based on a cutoff value of 3000 µm^3 in somatic volume obtained by the Nucleator) in the DNC was estimated by multiplying the density of the selected neurons by the volume of reference (Vref). Owing to the relatively small size of the DNC, a series of four equidistant Nissl-stained 30-µm-thick sections were obtained from each mouse (five mutant and five WT mice). The Vref was obtained using the Cavalieri principle (19,50).

Statistics

GraphPad software (GraphPad Prism 5; San Diego, CA, USA) was used to perform a two-way ANOVA with repeated measures between genotype and over time for the locomotor activity, rotarod and beam walking tests. An unpaired *t*-test was performed for the elevated plus maze, pole test, gait analysis, qPCR, catecholamine levels and western blot densitometry where genotype was the only variable. One-way ANOVA with Bonferroni's multiple comparison was used to analyze stereology and catecholamine level parameters. Statistical significance was deemed to be achieved if $P < 0.05$. Values are presented as mean ± SEM.

Supplementary Material

Supplementary Material is available at *HMG* online.

Conflict of Interest statement. None declared.

Funding

This work was supported by Bachmann-Strauss Dystonia and Parkinson Foundation; Dystonia Medical Research Foundation and National Institutes of Health NS081282 and RR026123.

References

1. Ledoux, M.S., Dauer, W.T. and Warner, T.T. (2013) Emerging common molecular pathways for primary dystonia. *Mov. Disord.*, **28**, 968–981.
2. Niethammer, M., Carbon, M., Argyelan, M. and Eidelberg, D. (2011) Hereditary dystonia as a neurodevelopmental circuit disorder: evidence from neuroimaging. *Neurobiol. Dis.*, **42**, 202–209.
3. Fuchs, T., Gavarini, S., Saunders-Pullman, R., Raymond, D., Ehrlich, M.E., Bressman, S.B. and Ozelius, L.J. (2009) Mutations in the THAP1 gene are responsible for DYT6 primary torsion dystonia. *Nat. Genet.*, **41**, 286–288.
4. Sengel, C., Gavarini, S., Sharma, N., Ozelius, L.J. and Bragg, D.C. (2011) Dimerization of the DYT6 dystonia protein, THAP1, requires residues within the coiled-coil domain. *J. Neurochem.*, **118**, 1087–1100.
5. Roussigne, M., Kossida, S., Lavigne, A.C., Clouaire, T., Ecochard, V., Glories, A., Amalric, F. and Girard, J.P. (2003) The THAP domain: a novel protein motif with similarity to the DNA-binding domain of P element transposase. *Trends Biochem. Sci.*, **28**, 66–69.
6. Clouaire, T., Roussigne, M., Ecochard, V., Mathe, C., Amalric, F. and Girard, J.P. (2005) The THAP domain of THAP1 is a large C2CH module with zinc-dependent sequence-specific DNA-binding activity. *Proc. Natl Acad. Sci. USA*, **102**, 6907–6912.

7. Cayrol, C., Lacroix, C., Mathe, C., Ecochard, V., Ceribelli, M., Loreau, E., Lazar, V., Dessen, P., Mantovani, R., Aguilar, L. *et al.* (2007) The THAP-zinc finger protein THAP1 regulates endothelial cell proliferation through modulation of pRB/E2F cell-cycle target genes. *Blood*, **109**, 584–594.
8. Vemula, S.R., Xiao, J., Zhao, Y., Bastian, R.W., Perlmutter, J.S., Racette, B.A., Paniello, R.C., Wszolek, Z.K., Uitti, R.J., Van Gerpen, J.A. *et al.* (2014) A rare sequence variant in intron 1 of THAP1 is associated with primary dystonia. *Mol. Genet. Genomic Med.*, **2**, 261–272.
9. Erogullari, A., Hollstein, R., Seibler, P., Braunholz, D., Koschmidder, E., Depping, R., Eckhold, J., Lohnau, T., Gillessen-Kaesbach, G., Grunewald, A. *et al.* (2014) THAP1, the gene mutated in DYT6 dystonia, autoregulates its own expression. *Biochim. Biophys. Acta*, **1839**, 1196–1204.
10. Sabogal, A., Lyubimov, A.Y., Corn, J.E., Berger, J.M. and Rio, D.C. (2010) THAP proteins target specific DNA sites through bipartite recognition of adjacent major and minor grooves. *Nat. Struct. Mol. Biol.*, **17**, 117–123.
11. Gervais, V., Campagne, S., Durand, J., Muller, I. and Milon, A. (2013) NMR studies of a new family of DNA binding proteins: the THAP proteins. *J. Biomol. NMR*, **56**, 3–15.
12. Neychev, V.K., Gross, R.E., Lehericy, S., Hess, E.J. and Jinnah, H.A. (2011) The functional neuroanatomy of dystonia. *Neurobiol. Dis.*, **42**, 185–201.
13. Liang, C.C., Tanabe, L.M., Jou, S., Chi, F. and Dauer, W.T. (2014) TorsinA hypofunction causes abnormal twisting movements and sensorimotor circuit neurodegeneration. *J. Clin. Invest.*, **124**, 3080–3092.
14. Gavarini, S., Cayrol, C., Fuchs, T., Lyons, N., Ehrlich, M.E., Girard, J.P. and Ozelius, L.J. (2010) Direct interaction between causative genes of DYT1 and DYT6 primary dystonia. *Ann. Neurol.*, **68**, 549–553.
15. Kaiser, F.J., Osmanoric, A., Rakovic, A., Erogullari, A., Uflacker, N., Braunholz, D., Lohnau, T., Orolicki, S., Albrecht, M., Gillessen-Kaesbach, G. *et al.* (2010) The dystonia gene DYT1 is repressed by the transcription factor THAP1 (DYT6). *Ann. Neurol.*, **68**, 554–559.
16. Schwenk, F., Baron, U. and Rajewsky, K. (1995) A cre-transgenic mouse strain for the ubiquitous deletion of loxP-flanked gene segments including deletion in germ cells. *Nucl. Acids Res.*, **23**, 5080–5081.
17. Srinivasan, K., Leone, D.P., Bateson, R.K., Dobreva, G., Kohwi, Y., Kohwi-Shigematsu, T., Grosschedl, R. and McConnell, S.K. (2012) A network of genetic repression and derepression specifies projection fates in the developing neocortex. *Proc. Natl Acad. Sci. USA*, **109**, 19071–19078.
18. Fink, A.J., Englund, C., Daza, R.A., Pham, D., Lau, C., Nivison, M., Kowalczyk, T. and Hevner, R.F. (2006) Development of the deep cerebellar nuclei: transcription factors and cell migration from the rhombic lip. *J. Neurosci.*, **26**, 3066–3076.
19. Sultan, F., Konig, T., Mock, M. and Thier, P. (2002) Quantitative organization of neurotransmitters in the deep cerebellar nuclei of the Lurcher mutant. *J. Comp. Neurol.*, **452**, 311–323.
20. Ortiz-Virumbrales, M., Ruiz, M., Hone, E., Dolios, G., Wang, R., Morant, A., Kottwitz, J., Ozelius, L.J., Gandy, S. and Ehrlich, M.E. (2014) Dystonia type 6 gene product Thap1: identification of a 50 kDa DNA-binding species in neuronal nuclear fractions. *Acta Neuropathol. Commun.*, **2**, 139.
21. Ishida, S., Huang, E., Zuzan, H., Spang, R., Leone, G., West, M. and Nevins, J.R. (2001) Role for E2F in control of both DNA replication and mitotic functions as revealed from DNA microarray analysis. *Mol. Cell. Biol.*, **21**, 4684–4699.
22. Tucker, K.L. (2001) Methylated cytosine and the brain: a new base for neuroscience. *Neuron*, **30**, 649–652.
23. Pascoli, V., Valjent, E., Corbille, A.G., Corvol, J.C., Tassin, J.P., Girault, J.A. and Herve, D. (2005) cAMP and extracellular signal-regulated kinase signaling in response to d-amphetamine and methylphenidate in the prefrontal cortex in vivo: role of beta 1-adrenoceptors. *Mol. Pharmacol.*, **68**, 421–429.
24. Schneider, S.A., Ramirez, A., Shafiee, K., Kaiser, F.J., Erogullari, A., Bruggemann, N., Winkler, S., Bahman, I., Osmanovic, A., Shafa, M.A. *et al.* (2011) Homozygous THAP1 mutations as cause of early-onset generalized dystonia. *Mov. Disord.*, **26**, 858–861.
25. Zhang, L., Yokoi, F., Jin, Y.H., DeAndrade, M.P., Hashimoto, K., Standaert, D.G. and Li, Y. (2011) Altered dendritic morphology of Purkinje cells in Dyt1 DeltaGAG knock-in and purkinje cell-specific Dyt1 conditional knockout mice. *PLoS One*, **6**, e18357.
26. Song, C.H., Bernhard, D., Hess, E.J. and Jinnah, H.A. (2014) Subtle microstructural changes of the cerebellum in a knock-in mouse model of DYT1 dystonia. *Neurobiol. Dis.*, **62**, 372–380.
27. Kwon, C.H., Zhu, X., Zhang, J. and Baker, S.J. (2003) mTor is required for hypertrophy of Pten-deficient neuronal soma in vivo. *Proc. Natl Acad. Sci. USA*, **100**, 12923–12928.
28. Rethinasamy, P., Muthuchamy, M., Hewett, T., Boivin, G., Wolska, B.M., Evans, C., Solaro, R.J. and Wieczorek, D.F. (1998) Molecular and physiological effects of alpha-tropomyosin ablation in the mouse. *Circ. Res.*, **82**, 116–123.
29. Minamisawa, S., Gu, Y., Ross, J. Jr, Chien, K.R. and Chen, J. (1999) A post-transcriptional compensatory pathway in heterozygous ventricular myosin light chain 2-deficient mice results in lack of gene dosage effect during normal cardiac growth or hypertrophy. *J. Biol. Chem.*, **274**, 10066–10070.
30. Wang, W., Bu, B., Xie, M., Zhang, M., Yu, Z. and Tao, D. (2009) Neural cell cycle dysregulation and central nervous system diseases. *Prog. Neurobiol.*, **89**, 1–17.
31. Wichmann, T. (2008) Commentary: dopaminergic dysfunction in DYT1 dystonia. *Exp. Neurol.*, **212**, 242–246.
32. Goodchild, R.E., Grundmann, K. and Pisani, A. (2013) New genetic insights highlight 'old' ideas on motor dysfunction in dystonia. *Trends Neurosci.*, **36**, 717–725.
33. Segawa, M. (2011) Dopa-responsive dystonia. *Handb. Clin. Neurol.*, **100**, 539–557.
34. Nicholas, A.P., Hokfelt, T. and Pieribone, V.A. (1996) The distribution and significance of CNS adrenoceptors examined with in situ hybridization. *Trends Pharmacol. Sci.*, **17**, 245–255.
35. Meitzen, J., Luoma, J.I., Stern, C.M. and Mermelstein, P.G. (2011) beta1-Adrenergic receptors activate two distinct signaling pathways in striatal neurons. *J. Neurochem.*, **116**, 984–995.
36. Srinivasan, J. and Schmidt, W.J. (2003) Potentiation of parkinsonian symptoms by depletion of locus coeruleus noradrenaline in 6-hydroxydopamine-induced partial degeneration of substantia nigra in rats. *Eur. J. Neurosci.*, **17**, 2586–2592.
37. Lindenbach, D., Ostock, C.Y., Eskow Jaunarajs, K.L., Dupre, K.B., Barnum, C.J., Bhide, N. and Bishop, C. (2011) Behavioral and cellular modulation of L-DOPA-induced dyskinesia by beta-adrenoceptor blockade in the 6-hydroxydopamine-lesioned rat. *J. Pharmacol. Exp. Ther.*, **337**, 755–765.
38. Ogawa, N., Mizukawa, K., Hirose, Y., Kajita, S., Ohara, S. and Watanabe, Y. (1987) MPTP-induced parkinsonian model in mice: biochemistry, pharmacology and behavior. *Eur. Neurol.*, **26**(Suppl 1), 16–23.

39. Richter, F. and Richter, A. (2014) Genetic animal models of dystonia: common features and diversities. *Prog. Neurobiol.*, **121C**, 91–113.
40. Page, M.E., Bao, L., Andre, P., Pelta-Heller, J., Sluzas, E., Gonzalez-Alegre, P., Bogush, A., Khan, L.E., Iacovitti, L., Rice, M.E. *et al.* (2010) Cell-autonomous alteration of dopaminergic transmission by wild type and mutant (DeltaE) TorsinA in transgenic mice. *Neurobiol. Dis.*, **39**, 318–326.
41. Balcioglu, A., Kim, M.O., Sharma, N., Cha, J.H., Breakefield, X.O. and Standaert, D.G. (2007) Dopamine release is impaired in a mouse model of DYT1 dystonia. *J. Neurochem.*, **102**, 783–788.
42. Song, C.H., Fan, X., Exeter, C.J., Hess, E.J. and Jinnah, H.A. (2012) Functional analysis of dopaminergic systems in a DYT1 knock-in mouse model of dystonia. *Neurobiol. Dis.*, **48**, 66–78.
43. Defazio, G., Berardelli, A. and Hallett, M. (2007) Do primary adult-onset focal dystonias share aetiological factors? *Brain*, **130**, 1183–1193.
44. Fasano, A., Nardocci, N., Elia, A.E., Zorzi, G., Bentivoglio, A.R. and Albanese, A. (2006) Non-DYT1 early-onset primary torsion dystonia: comparison with DYT1 phenotype and review of the literature. *Mov. Disord.*, **21**, 1411–1418.
45. Wu, Y., Wang, C., Sun, H., LeRoith, D. and Yakar, S. (2009) High-efficient FLPo deleter mice in C57BL/6J background. *PLoS One*, **4**, e8054.
46. Unterwald, E.M., Page, M.E., Brown, T.B., Miller, J.S., Ruiz, M., Pescatore, K.A., Xu, B., Reichardt, L.F., Beverley, J., Tang, B. *et al.* (2013) Behavioral and transcriptome alterations in male and female mice with postnatal deletion of TrkB in dorsal striatal medium spiny neurons. *Mol. Neurodegener.*, **8**, 47.
47. Brown, T.B., Bogush, A.I. and Ehrlich, M.E. (2008) Neocortical expression of mutant huntingtin is not required for alterations in striatal gene expression or motor dysfunction in a transgenic mouse. *Hum. Mol. Genet.*, **17**, 3095–3104.
48. Fleming, S.M. and Chesselet, M.F. (2006) Behavioral phenotypes and pharmacology in genetic mouse models of Parkinsonism. *Behav. Pharmacol.*, **17**, 383–391.
49. Paxinos, G. and Franklin, K.B.J. (2012) *The Mouse Brain in Stereotaxic Coordinates*, 4th edn. Academic Press, San Diego, Oct 25, Print Book ISBN: 9780123910578.
50. Schmitz, C. and Hof, P.R. (2005) Design-based stereology in neuroscience. *Neuroscience*, **130**, 813–831.